

# Simulation of field-aligned $H^+$ and $He^+$ dynamics during late-stage plasmasphere refilling

J. Krall<sup>1</sup>, J. D. Huba<sup>1</sup>, and J. A. Fedder<sup>2</sup>

<sup>1</sup>Plasma Physics Div., Naval Research Lab., Code 6790, 4555 Overlook Ave., SW, Washington, D.C., 20375-5346, USA

<sup>2</sup>Icarus Research, Inc., P.O. Box 30780, Bethesda, MD 20824-0780, USA

Received: 9 November 2007 – Revised: 7 March 2008 – Accepted: 30 April 2008 – Published: 11 June 2008

**Abstract.** The refilling of the plasmasphere for  $3 \leq L \leq 4$  following a model storm is simulated over long times (days) using the NRL ionosphere code SAMI2 (Sami2 is Another Model of the Ionosphere). Refilling is dependent on the supply of topside  $H^+$  and  $He^+$  ions with the result that  $H^+$  refilling rates decrease and  $He^+$  refilling rates generally increase with increasing  $F10.7$  index. Both early- and late-stage refilling are affected by net ion flows from the warmer to the colder geomagnetic hemisphere. When these flows are strong, the ability of the “winter helium bulge” to increase  $He^+$  refilling rates is suppressed. When neutral winds are not included, refilling rates fall, typically by a factor of two. In most cases, late-stage  $He^+$  refilling is proportional to  $H^+$  refilling, with typical  $He^+/H^+$  density ratios of 2% for solar minimum and 10% for solar maximum. For high values of  $F10.7$ ,  $He^+$  refilling exhibits a strong diurnal variation so that the  $He^+/H^+$  density ratio varies by as much as a factor of two during late-stage refilling. Finally if the plasmasphere is left undisturbed, the  $H^+$  density can refill for as long as five weeks at  $L=3$  and ten weeks at  $L=4$ , with saturation densities nearly an order of magnitude greater than typical observed densities. This confirms that the plasmasphere at these  $L$  values rarely obtains saturation.

**Keywords.** Ionosphere (Ionosphere-magnetosphere interactions; Modeling and forecasting) – Magnetospheric physics (Plasmasphere)

## 1 Introduction

The plasmasphere is a dynamic region of high-altitude space where plasma, primarily  $H^+$  and  $He^+$  ions, is held in place by the dipole field of the earth (Lemaire and Gringauz, 1998, and references therein). As the co-rotating plasmasphere

Correspondence to: J. Krall  
(jonathan.krall@nrl.navy.mil)

interacts with ionospheric and magnetospheric potentials, plasma can escape, emptying the contents of one or more “flux tubes” over a time scale of minutes. In effect, individual flux tubes can become “open,” so that the plasma escapes, or “closed,” so that the outflows from the topside ionosphere are once again trapped (Nishida, 1966). Observations of the ill-understood process of plasmasphere refilling indicate that it occurs on a time scale of days (see, e.g. review by Singh and Horwitz, 1992). The outward convection and opening of flux tubes, which occurs sunward of the plasmopause (Nishida, 1966), is greatly enhanced by geomagnetic activity and can cause significant global erosion of the plasmasphere (Carpenter, 1966; Song et al., 1988; Lockwood et al., 1990; Chi et al., 2005). It can also cause other observed phenomena, such as multiple plasmapauses in some sectors (Horwitz et al., 1990a; Sandel et al., 2001). Extreme ultraviolet (EUV) images of the  $He^+$  plasmasphere from the IMAGE satellite (Burch, 2000) show that the plasmopause radius can shrink by approximately one L-shell (from  $L=4$  to  $L=3$ ) in less than three hours (Goldstein et al., 2003).

In this paper we report on SAMI2 (Huba et al., 2000a) simulations of refilling dynamics for the  $H^+$  and  $He^+$  components of the plasmasphere. Comparisons of the  $H^+$  and  $He^+$  plasmaspheres are of interest because the extreme ultraviolet (EUV) imager on board the IMAGE satellite shows the  $He^+$  plasmasphere and its structure, which is generally assumed to correspond to that of the higher density  $H^+$  plasmasphere. However, observations show that  $He^+$  densities can exceed  $H^+$  densities during early-stage refilling (Horwitz et al., 1990a; Denton et al., 2002).

To our knowledge, this is the first presentation of dynamical refilling simulations in which both the  $H^+$  and  $He^+$  plasmaspheric populations have realistic ionospheric sources. This study differs from previous physics-based refilling simulations (Singh et al., 1986; Rasmussen and Schunk, 1988; Guiter and Gombosi, 1990; Tu et al., 2003; Singh and Horwitz, 1992, and references therein) in that both  $H^+$  and  $He^+$

are included, the source of plasmasphere ions is a comprehensive physics-based simulated ionosphere (see, e.g. Huba et al., 2000a,b, 2005), refilling is initiated with the simulated loss of high-altitude plasma taking place over a period of hours (to simulate a storm), the complete ion dynamics along the direction of the field are computed for all ion species (i.e. the inertial terms are included), and the field geometry uses a flexible dipole model of the earth's geomagnetic field that mimics the IGRF in the low- to mid-latitude ionosphere. While some of the past modeling work includes similar features, such as inertial ions (Guiter and Gombosi, 1990) or a realistic ionosphere (Guiter and Gombosi, 1990; Tu et al., 2003), none of them include all of these features.

That we use a tilted IGRF-like field geometry is significant in that it breaks the north-south symmetry that is common in past refilling simulations. Asymmetries are evident in the data, where upflow from the more strongly illuminated of the conjugate ionospheric sources can dominate on a given field line (Chandler and Chappell, 1986). Our present study supports the idea that flows from the more strongly illuminated geomagnetic hemisphere are significant, and even ubiquitous, affecting both early- and late-stage refilling dynamics.

### 1.1 Early and late stage refilling

Early theoretical work on the plasmasphere includes a number of theoretical studies to determine the properties of equilibrium plasmaspheric (Angerami and Thomas, 1964) and exospheric (Eviatar et al., 1964) flux tubes. Refilling calculations based on inflow rates from the base of a model exosphere (e.g. Banks et al., 1971; Lemaire, 1989) tend to produce refilling rates greater than those observed (Park, 1970). However, as Banks et al. (1971) speculated, refilling is a more complex process than first thought, with a supersonic early stage followed by a subsonic late stage.

At the present time, both the data (Park, 1970; Sojka and Wrenn, 1985; Song et al., 1988; Singh and Horwitz, 1992; Lawrence et al., 1999; Su et al., 2001; Tu et al., 2003) and the models show that for a given flux tube, refilling begins with high-speed upflows from the two conjugate ionospheric sources, followed by a process in which the plasma is trapped or thermalized and, lastly, by a fluid-like evolution over a number of days. In general, early stage refilling (inflow and trapping;  $t < 24$  h) proceeds at a lower rate than late stage refilling ( $> 24$  h) (Lawrence et al., 1999). However, reported late stage saturation times differ significantly among the various studies (see, e.g. Song et al., 1988). For example, analyses of the data give refilling time scales from 3 to 15 days (Rasmussen et al., 1993; Lambour et al., 1997; Lawrence et al., 1999; Su et al., 2001) at geosynchronous orbit ( $6.6 R_E$ ), with results varying with season and with the solar cycle (Rasmussen et al., 1993). The range of observed refilling times, while broad, nevertheless contrasts with the modeling work of Rasmussen et al. (1993), who used past data and a

then-current model (Guiter and Gombosi, 1990) to find time scales in excess of 50 days at similar  $L$ -shells.

Much of the difference between the Lambour et al. (1997); Lawrence et al. (1999); Su et al. (2001) and the Rasmussen et al. (1993) time scales would seem to represent the difference between the observed dynamic plasmasphere (refilling continues until actual losses equal actual gains with details being missed by the relatively sparse measurements) and a quiescent model plasmasphere (refilling continues until the model plasmasphere saturates). While the situation is clouded by uncertainties in the observational data, the fact is that refilling has not been observed over such long time scales. To account for the fact that month-long refilling has not been observed, we hypothesize, as have others (Lemaire and Schunk, 1992), that loss and refilling processes occur often, or even continuously, over a sizable range of  $L$ -shell values, with the processes being most significant at a dynamic plasmopause. The results of the present study are consistent with this hypothesis.

### 1.2 One-fluid, two-fluid, and kinetic models

Results for early stage refilling simulations vary considerably from model to model. Hydrodynamic models are differentiated between one-fluid models (Singh et al., 1986; Guiter and Gombosi, 1990) and two fluid models (Rasmussen and Schunk, 1988; Singh et al., 1994), with the latter having separate fluids to distinguish northward and southward interhemispheric flows. During the initial inflow stage, these models produce shocks or shock-like behavior, with the shocks being above the equator in the one-fluid models and near the conjugate end-points in the two-fluid models.

For example, Rasmussen and Schunk (1988) used a two-fluid version of the single-fluid Singh et al. (1986) code to perform a two-fluid simulation of the same model refilling problem that was addressed by Singh et al. (1986). As expected, results from the two studies differ during early stage refilling, when shock-like flows are evident. After the first 12 h, however, the results are quite similar, with quantitative differences being of order 20% (see Fig. 5b, Singh et al., 1986; Rasmussen and Schunk, 1988, Fig. 10). These simulations included only H<sup>+</sup> ions with fixed-density ionospheric boundaries.

Two past fluid-model refilling studies (Guiter and Gombosi, 1990; Tu et al., 2003), are similar to the present work in that realistic ionospheric sources are included. Guiter and Gombosi (1990) include the ion momentum terms for their two hydrodynamic ion species (H<sup>+</sup> and O<sup>+</sup>) and include a realistic simulated ionosphere with several neutral and minor ion species. This work differs from the present study in that He<sup>+</sup> is not included, results are perfectly symmetric between the conjugate ionospheres, the initial depletions are relatively small ( $n/n_0 \geq 0.2$ ) and are instantaneous, and results are only reported for early stage refilling. Multi-day refilling results from this same code were reported by

Rasmussen et al. (1993, see Fig. 4 therein). While these were not elaborated upon, they do support the long refilling time scales determined by Rasmussen et al. (1993) and bear some similarities to our present results. Tu et al. (2003) describe refilling results from the field line interhemispheric plasma (FLIP) model (Richards and Wilkinson, 1998; St.-Maurice and Schunk, 1976). These simulations feature a tilted dipole geometry, a realistic ionosphere, and lengthy simulation times. However, the FLIP model solves a diffusive form of the momentum equation (i.e. the ion inertial terms are neglected), which is more appropriate for computing the quasi-equilibrium states that are reported by Tu et al. (2003) than the dynamical results that are of interest in the present study.

In order to study the early-stage trapping of plasma, kinetic models (particle electrons and ions) or semi-kinetic models (particle ions and fluid electrons) have been developed. These models typically include simplified ionospheric boundaries, allow the inclusion or non-inclusion of various physical effects such as coulomb collisions, wave-particle interactions, and temperature anisotropies, and vary in the specifics of the modeling of such details as thermodynamics and polarization electric fields (Lin et al., 1992; Wilson et al., 1992, 1993; Liemohn et al., 1999).

For example, Wilson et al. (1993) includes kinetic model ions that follow motion of physical ion gyro-centers along with fluid electrons. With only coulomb collisions thermalizing the ions, the  $L=4$  simulation transitions from distinct northward and southward inflows to a more fluid-like velocity distribution within 33 h. They also show that adding wave-particle heating and scattering increases the refilling rate during the first 12 h. This suggests that, with all scattering effects included, the transition from a kinetic to a fluid regime would occur more quickly. In fact, the dominant mechanism by which high-speed inflows from the conjugate ionospheres become thermalized may not yet have been identified (Wilson et al., 1992).

Of interest for the present study is the work of Singh et al. (1994), who performed a direct comparison between kinetic and two-fluid approaches to refilling along an  $L=4.5$  field line. As expected, results differ in the early stage, when flows are supersonic and shocks are in evidence in the fluid model. Once the flows become subsonic, however, refilling flow patterns and resulting densities are in good agreement. This result, along with the one- and two-fluid model comparison provided by Rasmussen and Schunk (1988), suggests that our present one-fluid model can be effectively used to study refilling, so long as we are careful to recognize that specific phenomena that occur during early-stage refilling may not be correct. More to the point, that the various approaches produce similar results (differences are of order 20%) after early-stage refilling supports our contention that our late-stage refilling results are both qualitatively and quantitatively valid.

In the present study, we focus on the refilling of the H<sup>+</sup> and He<sup>+</sup> plasmaspheres for  $3 \leq L \leq 4$ . We further consider a model “storm” in which plasma losses are imposed for as long as five hours, with the result that refilling flow patterns become established before actual refilling commences. We consider the significance, if any, of thermospheric coupling (neutral winds), EUV irradiances, and seasonal variations.

## 2 SAMI2 simulations

SAMI2 (Huba et al., 2000a) is a two-dimensional, physics-based model of the ionosphere. SAMI2 models the plasma and chemical evolution of seven ion species (H<sup>+</sup>, He<sup>+</sup>, N<sup>+</sup>, O<sup>+</sup>, N<sub>2</sub><sup>+</sup>, NO<sub>2</sub><sup>+</sup> and O<sub>2</sub><sup>+</sup>). Two features of SAMI2 that make it suitable for plasmaspheric studies are (1) the model includes ion inertia along the geomagnetic field so that it captures certain essential features of collisionless physics (e.g. ion sound waves) at high altitude, and (2) the model includes oxygen, hydrogen and helium ions on an equal footing. To our knowledge SAMI2 is the only ionosphere code that models full plasma transport for all of these ion species, including the molecular ions. The complete ion temperature equation is solved for three ion species (H<sup>+</sup>, He<sup>+</sup> and O<sup>+</sup>) and the electron temperature equation is solved. SAMI2 includes 21 chemical reactions and radiative recombination. In the current version of SAMI2, the neutral composition and temperature are specified using the empirical NRLMSISE00 model (Picone et al., 2002), that is based on MSIS86 (Hedin et al., 1991), and the neutral wind is specified using the HWM model (Hedin, 1987).

SAMI2 uses a flexible dipole model of Earth’s geomagnetic field: in the low- to mid-latitude ionosphere it mimics the IGRF by fitting a dipole field to IGRF at each longitude in the grid while at high latitude it uses a standard tilted dipole. The nonorthogonal, nonuniform, fixed grid is closed so that there are no open field lines in the high latitude ionosphere that require specified boundary conditions. The plasma is transported transverse to the geomagnetic field using a finite volume method in conjunction with the donor cell method. At present, the latitudinal extent of SAMI2 is  $\pm 89^\circ$  and the altitude range is up to  $\sim 8 R_E$ . The simulations in this study assume closed dipole field lines and are limited to  $L$  values  $L < 4$ , where each SAMI2 field line is assumed to correspond to constant  $L$  (McIlwain, 1966).

### 2.1 The SAMI2 plasmasphere

The version used here is the open-source version of the SAMI2 code (Huba and Joyce, 2002, see <http://wwwppd.nrl.navy.mil/sami2-OSP/>) with the initial conditions modified at high altitude ( $>4000$  km) and with the addition of a simple storm-time loss function. Because co-rotational forces have not yet been added to the SAMI2 code (in the present version of SAMI2, the Sun rotates around the Earth), we have

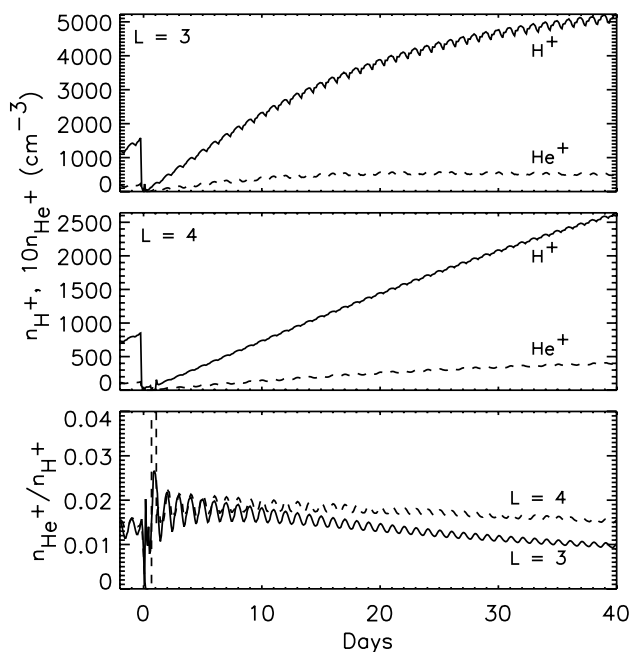


**Fig. 1.** H<sup>+</sup> and He<sup>+</sup> densities versus time following a model storm, with the He<sup>+</sup> density scaled up by a factor of 10, for longitude 0, winter, and moderate solar activity. Densities are given at the magnetic equator for  $L=3$  (top panel) and  $L=4$  (middle panel). He<sup>+</sup>/H<sup>+</sup> density ratios are also plotted (bottom panel).

limited these simulations  $L \leq 4$ , where mechanical forces associated with co-rotation are small in comparison to gravitational forces (the ratio of these forces is everywhere  $\leq 22\%$ , peaking at the  $L=4$  magnetic apex).

The present study does not include a model magnetosphere, a model solar wind, or their potential fields. As such we limit our results to the consideration of the refilling of the H<sup>+</sup> and He<sup>+</sup> components of the  $3 \leq L \leq 4$  plasmasphere following a significant plasma loss. For simplicity, and consistent with the lack of other potentials that would drive cross-field drifts, we exclude  $\mathbf{E} \times \mathbf{B}$  drifts in the results below.

One of the dimensions of the non-orthogonal SAMI2 grid corresponds to points following field lines at a fixed longitude. The transverse grid corresponds to steps from field line to field line (or L-shell to L-shell), again at fixed longitude. In these simulations, we used a grid with 200 points per field line, and with the variable grid parameters set to provide high resolution at high altitude. In our simplest cases, we reduced the transverse grid to three closely-spaced field lines, effectively creating a one dimensional simulation of a single L-shell at fixed longitude. For most of the two-dimensional runs, we used a grid with 21 field lines between  $L=2.9$  and  $L=4.1$  and 200 grid points per field line.

We have performed a number of single-field-line simulations and find saturated H<sup>+</sup> densities as large as  $5000 \text{ cm}^{-3}$  at  $L=3$  and  $3500 \text{ cm}^{-3}$  at  $L=4$ , above the magnetic equator.

Observations (Carpenter, 1966; Horwitz et al., 1990a; Su et al., 2001) show that the differences between these values and more typical numbers –  $1000 \text{ cm}^{-3}$  at  $L=3$  and  $500 \text{ cm}^{-3}$  at  $L=4$  (Corcuff et al., 1972; Horwitz et al., 1990b; Tu et al., 2006; Rasmussen and Schunk, 1990, and references therein) – lie in the dynamic nature of the plasmasphere. That is, these simulations correspond to a prolonged quiet period and, further, do not include a steady-state loss function such as the plasmaspheric wind of Lemaire and Schunk (1992). Neither are they coupled to a model magnetosphere in order to compute these losses self-consistently. Similarly, our long-term simulations show that saturated  $L=3$  He<sup>+</sup> densities, in excess of  $500 \text{ cm}^{-3}$ , are similarly larger than observed values of about  $200 \text{ cm}^{-3}$  (Horwitz et al., 1990b).

In all cases we initiate the pre-storm model plasmasphere with densities based on observations rather than saturated values. In all cases the initial H<sup>+</sup> density is  $1000 \text{ cm}^{-3}$  at the  $L=3$  magnetic apex with a linear reduction versus altitude down to  $500 \text{ cm}^{-3}$  at the  $L=4$  magnetic apex, and the with the He<sup>+</sup>/H<sup>+</sup> density ratio set to 2%. We will see below that this value of the He<sup>+</sup>/H<sup>+</sup> density ratio is appropriate for solar minimum conditions. Because we have excluded cross-field drifts in the present study, dynamics along each field line are independent of neighboring field lines. As a result, these simulations are insensitive to pre-storm plasmaspheric densities. Nevertheless, we ran each simulation for 60 h (3 days and 2 nights) to allow initial transients to settle out before initiating a model storm.

Figure 1 shows long-time-scale refilling at the apex of the  $L=3$  and the  $L=4$  field line following a model plasma loss, or “storm” (the plasma loss function is described below). These results correspond to zero longitude, winter solstice, and moderate solar activity ( $F10.7$  index= $F10.7A=100$ , where  $F10.7A$  is the 81-day average of  $F10.7$ ). The early-stage fluctuations (days 0 to 1) in Fig. 1 and in similar figures below should be considered spurious; additional simulations show them to be sensitive to both physical and numerical parameters.

We believe that the long-term result shown in Fig. 1 is moot in the specific sense that our simulated plasmasphere is allowed to refill without further disturbance for a very long time following the model storm. Additional simulations show that, if the plasmasphere is left undisturbed, H<sup>+</sup> refilling can continue for as long as 5 weeks at  $L=3$  and 10 weeks at  $L=4$  without fully saturating. The  $L=4$  late-stage refilling rates for H<sup>+</sup>,  $73 \text{ cm}^{-3} \text{ day}^{-1}$ , and He<sup>+</sup>,  $1.4 \text{ cm}^{-3} \text{ day}^{-1}$ , which are based on refilling from 2 through 6 days after the model storm, are consistent with observations (Singh and Horwitz, 1992), as is the He<sup>+</sup>/H<sup>+</sup> density ratio (Horwitz et al., 1990b). At  $L=4$  we recover the result of Park (1970), who stated that the refilling time in the  $3.5 < L < 4.5$  range is approximately 8 days. Specifically, Fig. 1 (middle panel) shows that after 8 days of refilling, typical plasmaspheric densities (i.e. pre-storm values for these simulations) are obtained.

### 2.2 Plasmasphere loss function

A simple model function is used simulate a plasma loss, which we refer to as a “storm”. Here, plasma density is removed in small, discrete steps without changing other plasma parameters, such as temperature or velocity. The five-minute duration between steps is chosen to be long compared to the simulation time step (typically 1 to 10 s) and shorter than the time scale for significant erosion of the plasmasphere (tens of minutes up to hours). The intent is to allow the simulation to recover self-consistency during the period between density reductions.

In each stepwise density reduction, the density of every ion, if present, is reduced by a factor of 0.83. With reductions occurring once per 5 min, and in the absence of flows or other density sources, this factor reduces all densities by an order of magnitude per hour. The plasma loss function is applied over a long-enough time to significantly reduce the density (5 h) but with no ion densities being reduced to below an imposed minimum value of 1 cm<sup>-3</sup>. Typically, the loss function is fully applied above a selected L-shell value and above an altitude of 5000 km. Below this altitude, losses on affected field lines are reduced smoothly such that there are no losses below 1000 km. In all cases, we ensure that this loss function does not force the H<sup>+</sup> density to fall unphysically fast versus altitude. Specifically, H<sup>+</sup> is not allowed to decrease more rapidly than the rate dictated by the O<sup>+</sup> scale height and the O<sup>+</sup>+H→O+H<sup>+</sup> charge exchange reaction.

To ensure that the specifics of our ad hoc loss function were not affecting the results, we performed additional simulations. Here, we varied the loss-function duration, rate, height along the field line where the loss function begins, and height along the field line where the loss function becomes fully effective. We found that late-stage refilling rates were insensitive to these parameters. For example, while increasing the loss rate and/or decreasing the storm duration by a factor of two did change late-stage refilling rates, these changes were less than 10% in all cases.

### 3 Simulation results

We have performed a number of simulations for moderate ( $F10.7=F10.7A=100$ ) and high ( $F10.7=F10.7A=200$ ) solar activity (below we refer to these as “solar minimum” and “solar maximum”) at the time of the summer solstice, winter solstice, spring equinox and fall equinox. While most of our results are for longitude 0, similar sets of runs at longitudes 90 and 270 degrees were also performed.

The action of a model storm is illustrated in Fig. 2, which shows contour plots of the electron density before the model storm (panel a), at the end of the model storm (panel b), one day later (panel c), and two days later (panel d). In the typical case, the simulated region extends from  $L=2.9$  to  $L=4.1$ , with 21 transverse grid points (field lines) and 16 grids ly-

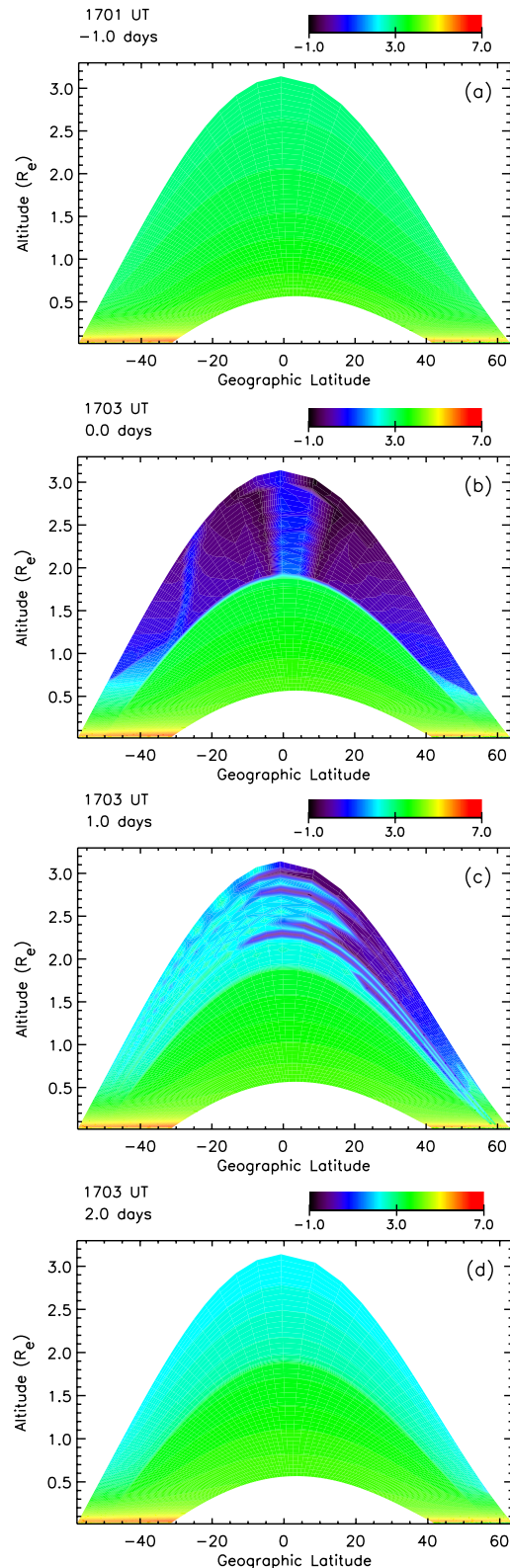


**Fig. 2.** Contour plots of the electron density (logarithmic) as a function of latitude and altitude: (a) pre-storm, (b) post storm, (c) one day after the storm, and (d) two days after the storm.

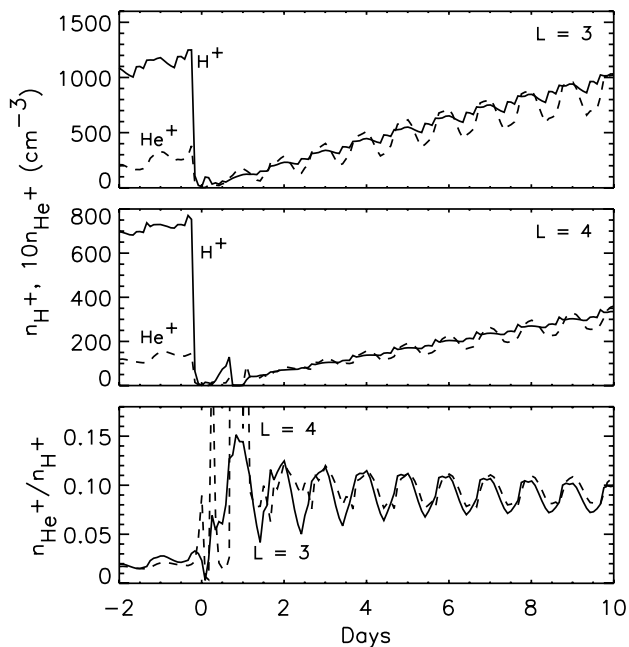


**Fig. 3.** H<sup>+</sup> and He<sup>+</sup> densities versus time, with the He<sup>+</sup> density scaled up by factor of 10, for longitude 0, winter, and high solar activity. Densities are given at the magnetic equator for  $L=3$  (top panel) and  $L=4$  (middle panel). He<sup>+</sup>/H<sup>+</sup> density ratios are also plotted (bottom panel).

ing in the  $3 \leq L \leq 4$  range. For Fig. 2, the simulated region is extended to  $1.6 \leq L \leq 4.1$  with additional field lines included to illustrate the contrast between refilling ( $L \geq 3$ ) and quietest regions. As in Fig. 1, this case corresponds to longitude 0, winter, and moderate solar activity. Thus, the spurious fluctuations versus time that occur shortly after the storm in Fig. 1 (these are most visible in the lower panel) correspond to those evident in Fig. 2b, c. As discussed in Sect. 1 above, past simulation studies suggest that late-stage refilling results are insensitive to the specifics of these spurious early-stage dynamics. Additional simulations show that this is indeed the case for this study.

Early-stage refilling results are nevertheless instructive. Specifically, Fig. 2c shows stronger refilling from the summer (southern) hemisphere than from the Northern Hemisphere in this case. We find that interhemispheric ion flows, coming from the more brightly illuminated of the magnetic hemispheres, are a common occurrence. This effect will be discussed further below. In this case (winter solstice, longitude 0), the interhemispheric ion flow is relatively weak: whereas the southern geographic hemisphere is more strongly lit, causing the flow, the magnetic equator is north of the geographical equator, reducing the affect of the southern summer on the southern magnetic hemisphere. The result, at the time of Fig. 2a, is a net northward velocity of order  $10 \text{ m s}^{-1}$  above the equator for  $3 < L < 4$ .

This relatively weak net velocity does little to disturb the symmetric inflow pattern during the storm itself as evidenced by the symmetric density pattern of Fig. 2b. Here, inflows exceed  $100 \text{ km s}^{-1}$ . This pattern, with a local peak at the magnetic equator, is reminiscent of past single-fluid refilling models, such as those of Singh et al. (1986, see Fig. 2 therein) and Guiter and Gombosi (1990, see Fig. 7 therein). In cases where the interhemispheric flow is much stronger, such as summer solstice at longitude 0 (where the magnetic geometry shifts the northern magnetic hemisphere towards northern summer), the inflow pattern is asymmetric and the density peak seen at the apex in Fig. 2b is pushed towards the the less-strongly illuminated southern magnetic hemisphere.

At later times, flow velocities are reduced, to order  $10 \text{ km s}^{-1}$  for Fig. 2c. For Fig. 2d, interhemispheric velocities are of order  $1 \text{ km s}^{-1}$  or less, while inflows remain of order  $10 \text{ km s}^{-1}$  at altitudes of 2000–4000 km. Our late-stage interhemispheric velocities are consistent with observed flows of  $100\text{--}1000 \text{ m s}^{-1}$  that are associated with refilling (Chandler and Chappell, 1986).

### 3.1 Refilling rates versus solar activity

Refilling rates for the  $L=3$  and  $L=4$  field lines were obtained from the time sequences of Fig. 1 by fitting a line to five days of data, beginning 1.5 days after the storm. Rates for intermediate field lines were also obtained. Here, the late-stage refilling rates for H<sup>+</sup> are  $240 \text{ cm}^{-3} \text{ day}^{-1}$  and  $73 \text{ cm}^{-3} \text{ day}^{-1}$  for  $L=3$  and  $L=4$ , respectively. For He<sup>+</sup> the rates are  $4.3 \text{ cm}^{-3} \text{ day}^{-1}$  and  $1.4 \text{ cm}^{-3} \text{ day}^{-1}$  for  $L=3$  and 4. As suggested in Fig. 1, He<sup>+</sup> refilling closely tracked H<sup>+</sup> refilling, with the density ratio for the first several days being approximately 2%. These results are typical of our simulations of solar minimum conditions.

A typical result for high solar activity is shown in Figs. 3 and 4. Here, the simulated conditions are otherwise the same as those of Figs. 1 and 2. As observed (Rasmussen et al., 1993; Lawrence et al., 1999; Richards et al., 2000; Su et al., 2001), the refilling rate for H<sup>+</sup> decreases with increasing solar activity. Here the rates are  $100 \text{ cm}^{-3} \text{ day}^{-1}$  and  $33 \text{ cm}^{-3} \text{ day}^{-1}$  for  $L=3$  and 4. By contrast, He<sup>+</sup> refilling rates increase with solar activity, increasing to  $9.3 \text{ cm}^{-3} \text{ day}^{-1}$  and  $3.0 \text{ cm}^{-3} \text{ day}^{-1}$ .

### 3.2 H<sup>+</sup> and He<sup>+</sup> concentrations

For moderate solar activity, Fig. 1, He<sup>+</sup> refilling closely tracked H<sup>+</sup> refilling, with a typical density ratio being 2%. For high solar activity, Figs. 3 and 4, He<sup>+</sup> refilling again closely tracked H<sup>+</sup> refilling, with an He<sup>+</sup>/H<sup>+</sup> density ratio of approximately 10%. In all cases, results were insensitive to pre-storm plasmaspheric densities. In the case shown in Fig. 3, for example, the pre-storm He<sup>+</sup>/H<sup>+</sup> density ratio is characteristic of solar minimum conditions (see, e.g. Fig. 1) while the post storm density ratio is characteristic of solar

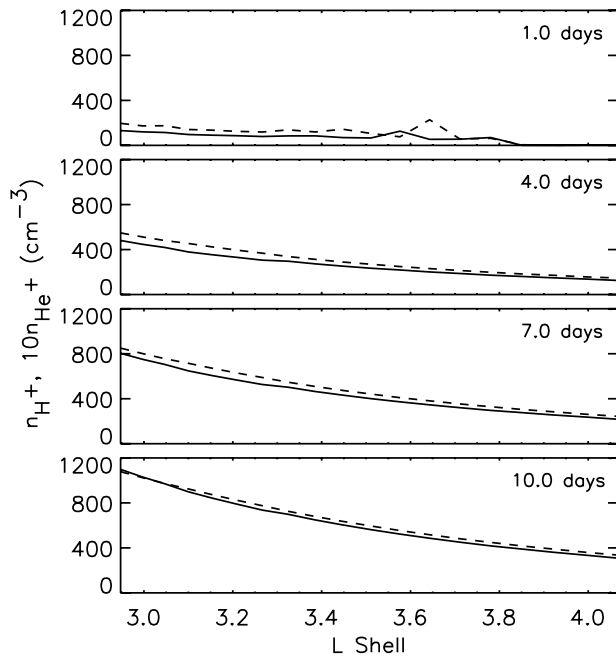


**Fig. 4.** H<sup>+</sup> (solid line) and He<sup>+</sup> (dashed line) densities versus L-shell at the magnetic equator, with the He<sup>+</sup> density scaled up by a factor of 10, for various times after the storm.

maximum conditions. That He<sup>+</sup> refilling closely tracks H<sup>+</sup> refilling versus both time and L-shell is clearly illustrated in Fig. 4, where  $n_{H^+}$  and  $10n_{He^+}$  are plotted versus  $L$  at various times after the storm. In this and other runs at high solar activity, He<sup>+</sup> refilling exhibits a strong diurnal variation, presumably due to photo-ionization of helium. This diurnal variation is largely absent from the H<sup>+</sup> curves.

To obtain a comparison between these simulations and the results of Denton et al. (2002), who found He<sup>+</sup>/H<sup>+</sup> density ratios exceeding unity in the winter-hemisphere topside ionosphere during refilling, we plotted (not shown) H<sup>+</sup> and He<sup>+</sup> concentrations at an altitude of 900 km, 11–50 h after the storm for the run shown in Figs. 3 and 4. We found winter-hemisphere He<sup>+</sup>/H<sup>+</sup> density ratios exceeding unity at all times. In the corresponding solar minimum case, however, He<sup>+</sup>/H<sup>+</sup> density ratios exceeding unity were only found during the dawn period, when diurnal variations favor He<sup>+</sup>.

Barring diurnal variations, He<sup>+</sup> refilling closely tracked H<sup>+</sup> refilling in most cases. For the longitude 0 runs, the one exceptional case occurred at the summer solstice for high solar activity. Here, the density ratio varied from 12% at  $L=4$ , two days after the storm, to 4% at  $L=3$ , after several days of refilling. This is illustrated in Fig. 5, where the He<sup>+</sup>/H<sup>+</sup> density ratio is plotted versus both time and L-shell.

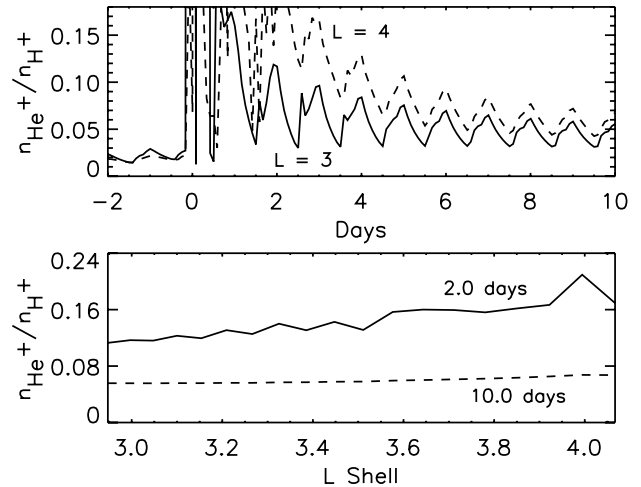


**Fig. 5.** He<sup>+</sup>/H<sup>+</sup> density ratio at the magnetic equator plotted versus time for  $L=3$  and  $L=4$  (top) and plotted versus L-shell for 2 days and 10 days after the storm (bottom). This simulation corresponds to longitude 0, summer, and high solar activity.

### 3.3 Interhemispheric ion flows

Figures 3 and 5 provide an example of the affect of inter-hemispheric ion flows on refilling rates. In Fig. 3 the net H<sup>+</sup> flow is northward and relatively weak. In Fig. 5, this flow is stronger and towards the south. As a result, the effect of the winter helium bulge is suppressed in Fig. 5, where the asymptotic He<sup>+</sup>/H<sup>+</sup> density ratio is about 0.04, relative to Fig. 3, where the density ratio is about 0.09. This difference is more dramatic in the late-time He<sup>+</sup> refilling rates, which drop from  $9.3 \text{ cm}^{-3} \text{ day}^{-1}$  and  $3.0 \text{ cm}^{-3} \text{ day}^{-1}$  for  $L=3$  and 4 in Fig. 3, to  $3.1 \text{ cm}^{-3} \text{ day}^{-1}$  and  $0.64 \text{ cm}^{-3} \text{ day}^{-1}$  for the case of Fig. 5. We believe that a stronger interhemispheric flow for the case of Fig. 5 is also the cause of the stronger early-stage refilling fluctuations that are apparent in that figure.

A summary of our refilling results for longitude 0 is given in Fig. 6. Results for H<sup>+</sup>, including variations with solar conditions, are consistent with measured late-time refilling rates (Horwitz et al., 1990b; Rasmussen et al., 1993; Lawrence et al., 1999; Su et al., 2001; Tu et al., 2006). However, we find seasonal variations in H<sup>+</sup> refilling that differ from past results. Specifically, Rasmussen et al. (1993, see Fig. 7) suggests that seasonal variations are stronger at solar maximum than at solar minimum and, at solar maximum, are stronger for  $L=4$  than for  $L=3$ . Our results do not consistently support either of these hypotheses.

In general, the SAMI2 refilling rates reflect the fact that the supply of H<sup>+</sup> generally decreases with solar activity, through the increased recombination of O<sup>+</sup> with increased temperature, and the fact that He<sup>+</sup> concentrations generally increase with solar activity, through photo-ionization. They

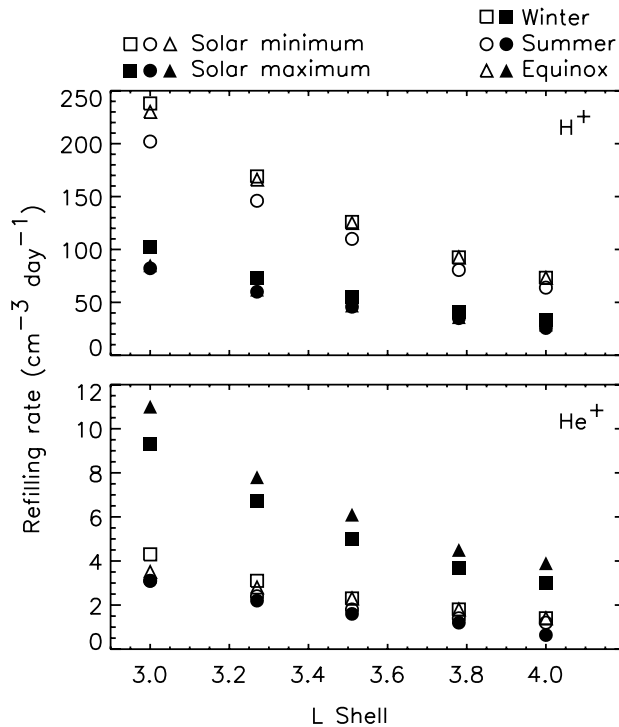


**Fig. 6.** Late-stage refilling rates for H<sup>+</sup> (top) and He<sup>+</sup> (bottom). All rates correspond to the magnetic equator and longitude 0.

also reflect the tendency of late-stage refilling to be strongly affected by flows from the hemisphere that is more strongly illuminated by the Sun. Because the more brightly lit hemisphere tends to have less H<sup>+</sup>, strong flows tend to reduce H<sup>+</sup> refilling rates.

In the case of He<sup>+</sup>, the winter helium bulge increases the He<sup>+</sup> supply in the less brightly lit hemisphere. However, the He<sup>+</sup> supply in the more brightly lit hemisphere also tends to increase because of photo-ionization. We find that strong flows tend to reduce He<sup>+</sup> refilling rates, suggesting that the significant effect of the winter helium bulge is suppressed when flows from the more brightly lit hemisphere are sufficiently strong. The strongest flows for longitude 0 occur at the summer solstice.

The effect of these interhemispheric ion flows is further illustrated by the comparison of the results at longitude 0, Fig. 6, to the results at longitude 270°, shown in Fig. 7. At longitude 0 the magnetic equator is north of the geographic equator, with the result that flows are strongest at the summer solstice (the Northern Hemisphere is more strongly lit, causing the southward flow, and the magnetic equator is north of the geographic equator enhancing the effect) and at solar maximum (where a high value of the time-averaged *F*10.7 index warms the northern thermosphere). For the solar maximum results, refilling rates are lower in the summer than in the winter in this case. At longitude 270°, Fig. 7, the mag-

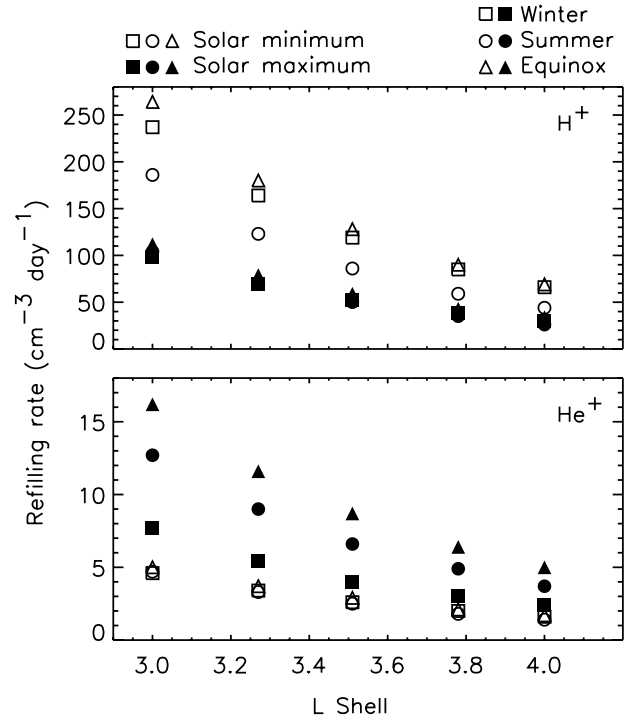


**Fig. 7.** Late-stage refilling rates for H<sup>+</sup> (top) and He<sup>+</sup> (bottom). All rates correspond to the magnetic equator and longitude 270°.

netic equator is south of the geographic equator and flows are strongest at the winter solstice and at solar maximum. For the solar maximum results, refilling rates are lower in the winter than in the summer in this case.

Finally, we note that winds strongly drive refilling in all cases. In runs where neutral wind velocities were set to zero, refilling rates dropped, typically by a factor of two.

#### 4 Conclusions

We have performed a number of SAMI2 simulations for moderate ( $F10.7=F10.7A=100$ ) and high ( $F10.7=F10.7A=200$ ) solar activity, at the time of the summer solstice, winter solstice, spring equinox and fall equinox. We have examined refilling of the plasmasphere following a model storm for  $3 \leq L \leq 4$  and have presented results at longitudes 0 and 270°.

During H<sup>+</sup> and He<sup>+</sup> refilling following a model storm, we find that the He<sup>+</sup>/H<sup>+</sup> density ratio is typically 2% for moderate solar activity (see Fig. 1) and 10% for high solar activity (see Figs. 3 and 4). At high solar activity, He<sup>+</sup> refilling exhibits a strong diurnal variation (about a factor of two), presumably due to photo-ionization of helium. As a result, the He<sup>+</sup>/H<sup>+</sup> density ratio is increased at dusk and reduced at dawn.

If left undisturbed, we find that the H<sup>+</sup> density can refill for as long as five weeks at  $L=3$  and ten weeks at  $L=4$ , with saturation densities nearly an order of magnitude larger than typical observed densities (see Fig. 1). However, evidence suggests that such field lines are rarely left undisturbed (Corcuff et al., 1972; Lemaire and Schunk, 1992). If true, loss and refilling mechanisms are a constant and necessary component of any physics-based model of the plasmasphere and plasmopause. Further work is required to correctly identify and model the most significant of these loss mechanisms.

Refilling rates and, consequently, He<sup>+</sup>/H<sup>+</sup> density ratios are affected by the supply of topside ionosphere H<sup>+</sup> and He<sup>+</sup> and by the degree to which these sources can flow into the plasmasphere. We find that refilling flows are strongly affected by net ion flows, particularly the prevailing flow from the more-strongly-illuminated to the less-strongly-illuminated geomagnetic hemisphere. When inter-hemispheric flows are particularly strong, they affect the “winter helium bulge” can be suppressed, significantly decreasing the late-stage He<sup>+</sup> refilling rate.

In general, the topside ionosphere H<sup>+</sup> supply is reduced with increasing solar activity. We also find that the topside ionosphere O<sup>+</sup> density in the 1000–5000 km altitude range is greater in the more brightly lit hemisphere and also increases with solar activity. This leads us to speculate that the tendency of O<sup>+</sup> to act as a diffusive barrier to H<sup>+</sup> upflow (Lemaire and Gringauz, 1998) is a significant effect in these simulations. The inverse dependence of H<sup>+</sup> refilling on solar activity is well known from past studies (Rasmussen et al., 1993; Lawrence et al., 1999; Richards et al., 2000; Su et al., 2001). That photo-ionization, controlled in these simulations by the  $F10.7$  index, is the primary source of He<sup>+</sup> also affects these results: in our runs with high  $F10.7$  indices, seasonal (winter helium bulge) and diurnal variations in He<sup>+</sup> are strengthened. In general, He<sup>+</sup> refilling increases with solar activity.

A major assumption in this study is the neglect of the  $\mathbf{E} \times \mathbf{B}$  drift motion of the plasma. This assumption is motivated by several factors. First, we wanted to focus solely on the physics of multi-ion species diffusion and motion along the geomagnetic field, and assess the relevant time scales and He<sup>+</sup>/H<sup>+</sup> ratios for this aspect of the refilling process. Second, to realistically model the impact of the  $\mathbf{E} \times \mathbf{B}$  drift on plasmasphere dynamics requires a self-consistent electric field determined by the solar wind/magnetosphere/ionosphere interaction. Third, the  $\mathbf{E} \times \mathbf{B}$  drift is both radial and longitudinal, necessitating a 3-D ionosphere/plasmasphere model. The complexity associated with the last two issues is beyond the scope of this paper. However, we intend to explore the impact of  $\mathbf{E} \times \mathbf{B}$  motion on plasmasphere refilling with the self-consistent SAMI3/RCM (Rice Convection Model) code (Huba et al., 2005) in the near future. With the coupled model, future work will include (a) magnetospheric convection, which may limit saturation densities at these L-shells, (b) co-rotation, which would be

necessary for accurate simulations at geosynchronous orbit and for comparisons to the relative wealth of data from that altitude (Sojka and Wrenn, 1985; Song et al., 1988; Singh and Horwitz, 1992; Su et al., 2001, and references therein), (c) consideration of the dependence of refilling on magnetospheric activity (see, e.g. Song et al., 1988), and/or (d) independent variations in the daily and average  $F10.7$  indices, so as to partially distinguish thermospheric heating effects from photo-ionization effects.

*Acknowledgements.* This work was supported by the Office of Naval Research.

Topical Editor M. Pinnock thanks J. Lemaire and another anonymous referee for their help in evaluating this paper.

## References

- Angerami, J. J. and Thomas, J. O.: The distribution of electrons and ions in the Earth's exosphere, *J. Geophys. Res.*, 69, 4537–4560, 1964.
- Banks, P. M., Nagy, A. F., and Axford, W. I.: Dynamical behavior of thermal protons in the mid-latitude ionosphere and magnetosphere, *Planet. Space Sci.*, 19, 1053–1067, 1971.
- Burch, J. L.: IMAGE mission overview, *Space Sci. Rev.*, 91, 1–14, 2000.
- Carpenter, D. L.: Whistler studies of the plasmopause in the magnetosphere. I: Temporal variations in the position of the knee and some evidence on plasma motions near the knee, *J. Geophys. Res.*, 71, 693–709, 1966.
- Chandler, M. O. and Chappell, C. R.: Observations of the flow of the H<sup>+</sup> and He<sup>+</sup> along magnetic field lines in the plasmasphere, *J. Geophys. Res.*, 91, 8847–8860, 1986.
- Chi, P. J., Russell, C. T., Foster, J. C., Moldwin, M. B., Engebretson, M. J., and Mann, I. R.: Density enhancement in plasmasphere-ionosphere plasma during the 2003 Halloween Superstorm: Observations along the 330th magnetic meridian in North America, *Geophys. Res. Lett.*, 32, L03S07, doi:10.1029/2004GL021722, 2005.
- Corcuff, P., Corcuff, Y., Carpenter, D. L., Chappell, C. R., Vigneron, J., and Kleimenova, N.: La plasmasphere en periode de recouvrement magnetique. Etude combinee des donnees des satellites OGO 4, OGO 5, et des sifflements recus au sol, *Ann. Geophys.*, 28, 679–696, 1972, <http://www.ann-geophys.net/28/679/1972/>.
- Denton, M. H., Bailey, G. J., Wilford, C. R., Rodger, A. S., and Venkatraman, S.: He<sup>+</sup> dominance in the plasmasphere during geomagnetically disturbed periods: 1. Observational results, *Ann. Geophys.*, 20, 461–470, 2002, <http://www.ann-geophys.net/20/461/2002/>.
- Eviatar, A., Lenchek, A. M., and Singer, S. F.: Distribution of density in an ion-exosphere of a nonrotating planet, *Phys. Fluids*, 7, 1775–1779, 1964.
- Goldstein, J., Sandel, B. R., Forrester, W. T., and Reiff, P. H.: IMF-Driven plasmasphere erosion of 10 July 2000, *Geophys. Res. Lett.*, 30, 1146, doi:10.1029/2002GL016478, 2003b.
- Guiter, S. M. and Gombosi, T. I.: The role of high-speed plasma flows in plasmaspheric refilling, *J. Geophys. Res.*, 95, 10427–10440, 1990.
- Hedin, A. E.: MSIS-86 thermospheric model, *J. Geophys. Res.*, 92, 4649–4662, 1987.

- Hedin, A. E., Biondi, M. A., Burnside, R. G., Hernandez, G., Johnson, R. M., Killeen, T. L., Mazaudier, C., Meriwether, J. W., Salah, J. E., Sica, R. J., Smith, R. W., Spencer, N. W., Wickwar, V. B., and Virdi, T. S.: Revised global model of the thermosphere winds using satellite and ground-based observations, *J. Geophys. Res.*, 96, 7657–7688, 1991.
- Horwitz, J. L., Comfort, R. H., and Chappell, C. R.: A statistical characterization of plasmasphere density structure and boundary locations, *J. Geophys. Res.*, 95, 7937–7947, 1990a.
- Horwitz, J. L., Comfort, R. H., Richards, P. G., Chandler, M. O., Chappell, C. R., Anderson, P., Hanson, W. B., and Brace, L. H.: Plasmasphere-ionosphere coupling 2. Ion composition measurements at plasmaspheric and ionospheric altitudes with modeling results, *J. Geophys. Res.*, 95, 7949–7959, 1990b.
- Huba, J. D., Joyce, G., and Fedder, J. A.: SAMI2 (Sami2 is Another Model of the Ionosphere): A New Low-Latitude Ionosphere Model *J. Geophys. Res.*, 105, 23 035–23 053, 2000a.
- Huba, J. D., Joyce, G., and Fedder, J. A.: Ion sound waves in the topside equatorial ionosphere, *Geophys. Res. Lett.*, 27, 3181–3184, 2000b.
- Huba, J. D., Joyce, G., Sazykin, S., Wolf, R., and Spiro, R.: Simulation study of penetration electric fields in the low- to mid-latitude ionosphere, *Geophys. Res. Lett.*, 32, L23101, doi:10.1029/2005GL024162, 2005.
- Huba, J. D. and Joyce, G.: Open Source Project to aid ionospheric research, *EOS Trans. AGU*, 83, 188–188, 2002.
- Lambour, R. L., Weiss, L. A., Elphic, R. C., and Thomsen, M. F.: Global modeling of the plasmasphere following storm sudden commencements, *J. Geophys. Res.*, 102, 24 351–24 368, 1997.
- Lawrence, D. J., Thomsen, M. F., Borovsky, J. E., and McComas, D. J.: Measurements of early and late time plasmasphere refilling as observed from geosynchronous orbit, *J. Geophys. Res.*, 104, 14 691–14 704, 1999.
- Lemaire, J.: Plasma distribution models in a rotating magnetic dipole and refilling of plasmaspheric flux tubes, *Phys. Fluids B*, 1, 1519–1525, 1989.
- Lemaire, J. and Schunk, R. W.: Plasmaspheric wind, *J. Atmos. Solar-Terr. Phys.*, 54, 467–477, 1992.
- Lemaire, J. and Gringauz, K. I.: *The Earth's Plasmasphere*, Cambridge University Press, New York, NY, 1998.
- Liemohn, M. W., Khazanov, G. V., Craven, P. D., and Kozyra, J. U.: Nonlinear kinetic modeling of early stage plasmaspheric refilling, *J. Geophys. Res.*, 104, 10 295–10 306, 1999.
- Lin, J., Horwitz, J. L., Wilson, G. R., Ho, C. W., and Brown, D. G.: A semikinetic model for early stage plasmasphere refilling 2. Effects of wave-particle interactions, *J. Geophys. Res.*, 97, 1121–1134, 1992.
- Lockwood, M., Cowley, S. W. H., and Freeman, M. P.: The excitation of plasma convection in the high-latitude ionosphere, *J. Geophys. Res.*, 95, 7961–7972, 1990.
- McIlwain, C. E.: Magnetic coordinates, *Space Sci. Rev.*, 5, 585–598, 1966.
- Nishida, A.: Formation of plasmopause, or magnetospheric plasma knee, by combined action of magnetospheric convections and plasma escape from the tail, *J. Geophys. Res.*, 71, 5669–5679, 1966.
- Park, C. G.: Whistler observations of the interchange of ionization between the ionosphere and protonosphere, *J. Geophys. Res.*, 75, 4249–4260, 1970.
- Picone, J. M., Hedin, A. E., Drob, D. P., and Aikin, A. C.: NRLMSISE-00 empirical model of the atmosphere: Statistical comparisons and scientific issues, *J. Geophys. Res.*, 107, 1468, doi:10.1029/2002JA009430, 2002.
- Rasmussen, C. E. and Schunk, R. W.: Multistream hydrodynamic modeling of interhemispheric plasma flow, *J. Geophys. Res.*, 93, 14 557–14 565, 1988.
- Rasmussen, C. E. and Schunk, R. W.: A three-dimensional time-dependent model of the plasmasphere, *J. Geophys. Res.*, 95, 6133–6144, 1990.
- Rasmussen, C. E., Guiter, S. M., and Thomas, S. G.: A two-dimensional model of the plasmasphere: refilling time constants *Planet. Space Sci.*, 41, 35–43, 1993.
- Richards, P. G. and Wilkinson, P. J.: The ionosphere and thermosphere at southern midlatitudes during the November 1993 ionospheric storm: a comparison of measurement and modeling, *J. Geophys. Res.*, 103, 9373–9389, 1998.
- Richards, P. G., Chang, T., and Comfort, R. H.: On the causes of the annual variation in the plasmaspheric electron density, *J. Atmos. Solar-Terr. Phys.*, 62, 935–946, 2000.
- St.-Maurice, J.-P. and Schunk, R. W.: Diffusion and heat flow equations for the mid-latitude topside ionosphere, *Planet. Space Sci.*, 25, 907–920, 1976.
- Sandel, B. R., King, R. A., Forrester, W. T., Gallagher, D. L., Broadfoot, A. L., and Curtis, C. C.: Initial results from the IMAGE Extreme Ultraviolet Imager, *Geophys. Res. Lett.*, 28, 1439–1442, 2001.
- Singh, N., Schunk, R. W., and Thiemann, H.: Temporal features of the refilling of a plasmaspheric flux tube, *J. Geophys. Res.*, 91, 13 433–13 454, 1986.
- Singh, N. and Horwitz, J. L.: Plasmasphere refilling: recent observations and modeling, *J. Geophys. Res.*, 97, 1049–1079, 1992.
- Singh, N., Wilson, G. R., and Horwitz, J. L.: Comparison of hydrodynamic and semikinetic treatments for plasma flow along closed field lines, *J. Geophys. Res.*, 99, 11 495–11 506, 1994.
- Sojka, J. J. and Wrenn, G. L.: Refilling of geosynchronous flux tubes as observed at the equator by GEOS 2, *J. Geophys. Res.*, 90, 6379–6385, 1985.
- Song, X., Gendrin, R., and Caudal, G.: Refilling process in the plasmasphere and its relation to magnetic activity, *J. Atmos. Terr. Phys.*, 50, 185–195, 1988.
- Su, Y.-J., Thomsen, M. F., Borovsky, J. E., and Lawrence, D. J.: A comprehensive survey of plasmasphere refilling at geosynchronous orbit, *J. Geophys. Res.*, 106, 25 615–25 629, 2001.
- Tu, J.-N., Horwitz, J. L., Song, P., Huang, X.-Q., Reinisch, B. W., and Richards, P. G.: Simulating plasmaspheric field-aligned density profiles measured with IMAGE/RPI: effects of plasmasphere refilling and ion heating, *J. Geophys. Res.*, 108, 1017, doi:10.1029/2002JA009468, 2003.
- Tu, J., Song, P., Reinisch, B. W., Green, J. L., and Huang, X.: Empirical specification of field-aligned plasma density profiles for plasmasphere refilling, *J. Geophys. Res.*, 111, A06216, doi:10.1029/2005JA011582, 2006.
- Wilson, G. R., Horwitz, J. L., and Lin, J.: A semikinetic model for early stage plasmasphere refilling 1. Effects of coulomb collisions, *J. Geophys. Res.*, 97, 1109–1119, 1992.
- Wilson, G. R., Horwitz, J. L., and Lin, J.: Semikinetic modeling of plasma flow on outer plasmaspheric field lines, *Adv. Space Res.*, 13, 107–116, 1993.